Quantitative Numerical Analysis of *g* Strain in the EPR of Distributed Systems and Its Importance for Multicenter Metalloproteins

W. R. HAGEN, D. O. HEARSHEN, L. J. HARDING,* AND W. R. DUNHAM

*Biophysics Research Division, Institute of Science and Technology, and *Computing Center, University of Michigan, Ann Arbor, Michigan 48109*

A method for simulation of inhomogeneously broadened EPR of metallo-proteins based on recent theoretical advances is surveyed critically in terms of efficiency and accuracy. From the quality of the experimental spectrum, minimal boundary conditions are established for the spatial integration over the *g*-strained polycrystal. Computational efficiency is achieved by generating the $S = \frac{1}{2}$ spectrum as an absorption in *g* space, reducing the number of molecular orientations computed by filtering mosaic artifacts from the Fourier-transformed spectrum, and generating the lineshape due to *g* strain from a tabulated distribution function. These techniques provide a reduction in computation time by some two orders of magnitude and make the data analysis of EPR of metalloproteins by minimization practical. The resulting simulation program is superior to current approaches in that it does not introduce artifactual multiplicities, and it is expected to require a smaller number of fitting parameters for the quantitative analysis of most cases. To illustrate its potential, the method is applied to EPR data from the iron–sulfur centers in NADH:Q oxidoreductase and in QH_2:ferricytochrome *c* oxidoreductase, clarifying existing controversies on the stoichiometries of these centers. © 1985 Academic Press, Inc.

INTRODUCTION

The electron paramagnetic resonance spectrum of metallo-proteins is usually broadened inhomogeneously by a frequency-proportional mechanism known as *g* strain. The complexity of the mathematical description of this phenomenon (cf. the preceding paper (*1*)) invalidates current procedures (cf. (*2–3*)) of data reduction. In this paper, a series of techniques for the efficient computation of "*g*-strained" spectra based on a number of simplifying approximations are presented. The resulting reduction in computation time for simulation of EPR spectra makes the rigorous analysis of complex spectra arising from multicenter preparations by minimization practical.

For a randomly oriented, magnetically isolated system of effective spin $S = \frac{1}{2}$, the inhomogenously broadened EPR spectrum can be described (*4*) by

$$s(B) = \Omega^{-1} \iint_{\Omega B} f'(B) d\Omega dB. \tag{1}$$

233

The outer integration, over the surface of a sphere with area Ω, describes the probability that a unit vector $\mathbf{n}$ along the external magnetic field $\mathbf{B}$ is at polar angles θ, ϕ relative to the g tensor axis system of an arbitrary element in a grand ensemble of centers. The inner integration accounts for the resonance lineshape for a given orientation. Analytic solutions to Eq. [1] have been derived only for a few cases of high symmetry (5) but are not relevant to actual situations in proteins.

For one orientation, the resonance line with direction cosines l_x, l_y, l_z with respect to $\mathbf{B}$ is characterized by four quantities: position, intensity, width, and shape. The position is defined by the spectroscopic splitting factor

$$g = \left(\sum_{i=1}^{3} l_i^2 g_i^2\right)^{1/2} \tag{2}$$

in the effective resonance condition

$$\bar{B} = h\nu_0/(g\beta). \tag{3}$$

The intensity in frequency space (or in g space) has been derived for an oscillating magnetic field polarized perpendicular to $\mathbf{B}$ by several authors ((2) and references quoted therein). The algorithm of Isomoto $et\ al.$ (6),

$$I_g = \sum_{i=1}^{3} (g_i^2 - g^{-2}l_i^2 g_i^4), \tag{4}$$

involves the least number of arithmetic operations in the integration of Eq. [1]. As noted in (2), the intensity in field space is obtained by correcting with a factor $(dB/d\nu)$ so that, from Eqs. [3] and [4],

$$I_B = g^{-1}I_g. \tag{5}$$

The width in g space from g strain is a function of 4×3 spectral parameters

$$\sigma_{g|l_x l_y l_z} = f(g_1, g_2, g_3, \sigma_1, \sigma_2, \sigma_3, r_{12}, r_{23}, r_{31}, \alpha, \beta, \gamma), \tag{6}$$

three g values, three standard deviations of the elements of the tensorial quantity $\mathbf{p}$ that causes g strain, three associated correlation coefficients, and three angles defining the orientation of the p tensor with respect to the g tensor. Explicit expressions for σ_g were derived in the preceding paper (1).

The actual shape function in B shape will be skewed because the distribution observed as line broadening is from a random variable in g space. For a normally distributed spectroscopic splitting factor, Strong (7) derived the observable shape as

$$f'(B) = \frac{\bar{B}^2}{(2\pi(\Delta B)^2)^{1/2}} \left[\frac{-2}{B^3} + \frac{\bar{B}^4}{B^4(\Delta B)^2}\left[\frac{1}{B} - \frac{1}{\bar{B}}\right]\right]\exp\left[\frac{-\bar{B}^4}{2(\Delta B)^2}\left[\frac{1}{B} - \frac{1}{\bar{B}}\right]^2\right], \tag{7}$$

where $\bar{B}$ is the resonance field and ΔB is the equivalent of a standard deviation in field space. Although developed in terms of a normal distribution in g, our results are applicable for any distribution function.

The numerical integration of Eq. [1] takes the form of two nested loops. The outer loop, commonly referred to as the "powder loop," is a double loop because it runs over the direction cosines in terms of the polar angles θ and ϕ. It contains

the computation of position, intensity, and width, e.g., Eqs. [2]–[6], based on the parameters g_i, σ_i, and r_{ij} and the three angles α, β, and γ. The inner loop involves the computation of the lineshape by sampling on a mesh in magnetic field; the truncation points for the sampling range are chosen to be 0.1% of peak intensity.

Typically, about 90% of the computer time involved in this integration is expended in the inner loop so that the total time is roughly the inner-loop time times the number of orientations in the powder loop. To obtain a smooth spectrum, the number of solid-angle steps must be large enough to average the mosaic artifacts. This computation is practical because most researchers make the oversimplifying assumptions that the distribution function is symmetric in B and, more importantly, that the linewidth tensor is collinear with g. Further, minimization of the difference between the simulated spectrum and the data has been based on obtaining an "appealing" result by visual inspection.

Recent advances in the theory of g strain, however, have made this linewidth algorithm more complex and, therefore, more time consuming. Moreover, an even more substantial increase in computation time is dictated by the possible occurrence of (near-) zero-strain orientations (8), i.e., orientations for which, as a consequence of negative correlation, σ_g is less than the linewidths at the principal-axis orientations by over an order of magnitude. To overcome mosaic-artifact ripples, the number of steps in both the polar angles θ, ϕ must be raised by about an order of magnitude. Thus integration time increases by two orders of magnitude so that simulation based on visual inspection becomes a tedious and costly undertaking and actual minimization is impractical.

The techniques delineated below reduce the integration time by about two orders of magnitude without any significant loss in accuracy.

POWDER-INTEGRATION BOUNDARIES

In the integration over phase space, three basic spectral quantities are calculated: the resonance position, $\bar{B}$, the intensity, I_g, and the variance of g strain, σ_g^2. The minimal limits of integration are dictated by symmetry or by the periodicity of the functions of the spectral parameters. Alternatively, ignoring periodicity, one can integrate over the surface of the sphere provided that, for the eightfold sets of potentially equivalent points in all octants (e.g., (θ, ϕ) and $(\pi - \theta, \pi - \phi)$, etc.), only one occurs in the integration. This can be accomplished by careful choice of the starting point of integration, $(\cos \theta_1, \phi_1)$ and of the incremental steps $d \cos \theta$ and $d\phi$. If m_θ and m_ϕ, which must be odd, are the number of incremental steps in $\cos \theta$ and ϕ, respectively, then

$$d \cos \theta = -2/m_\theta$$

$$\cos \theta_1 = 1 - 3/(2m_\theta)$$

$$d\phi = 2\pi/m_\phi$$

$$\phi_1 = (7/8)d\phi. \tag{8}$$

The points of evaluation generated by Eq. [8] correspond to mid-point integration for a uniformly spaced mesh that accounts for periodicity. The integration over the

whole sphere is as accurate and no more time-consuming than the integration over a periodic subsurface (as long as the period is not less than $\pi/2$).

The second condition delimiting the powder integration is the number of computed molecular orientations, $m_\theta m_\phi$. This number should be as small as possible (because computation time is directly proportional to it) consistent with the required accuracy. A typical EPR sample of a frozen solution of metalloproteins contains 10^{-8} mol of sites; data substantiate the hypothesis that, even in ice polycrystals, protein-molecular orientation is random. Typically, however, the number of computed orientations is between 10 and 10^5.

If the number of orientations is too small, the spectrum will be resolved from individual orientations, i.e., computer-mosaic rippling. Theoretically, mosaic rippling can be eliminated numerically by computing a sufficiently large number of orientations. A typical simulation of a [2Fe–2S] ferredoxin is shown in Fig. 1. The purely g-strained spectrum was obtained by taking a fully deuterated and fully ^{56}Fe substituted protein and by measuring at a relatively high microwave frequency to avoid interference from unresolved (super)hyperfine splittings.
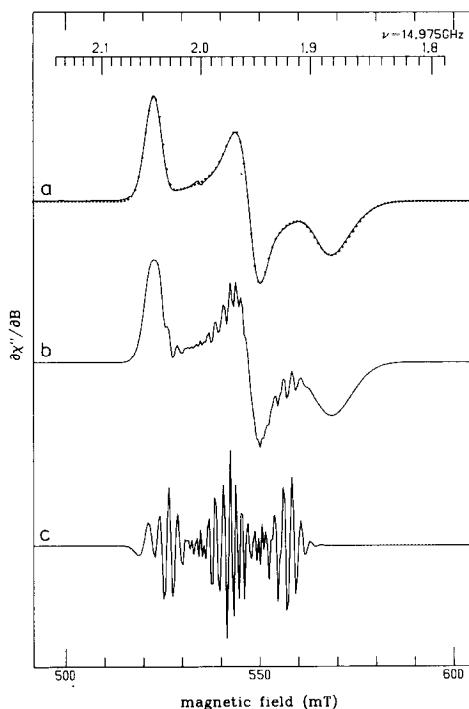

FIG. 1. Rippling simulation reflecting mosaic artifacts as a result of the computation of too low a number of molecular orientations: (a) solid trace, experimental P-band spectrum of ^{2}H, $[2^{56}Fe-2S]^{1+(2+;1+)}$ ferredoxin from *S. lividus;* dotted trace, near-ideal simulation based on 301×299 orientations, (b) noisy simulation based on 41×39 orientations, and (c) difference spectrum ($\times 4$). Simulation parameters: $g_{1,2,3}$ = 1.881, 1.959, 2.051; $\sigma_{1,2,3}$ = 0.0254, 0.0060, 0.0130; $r_{12,23,31}$ = 1.00, −0.91, −1.00; α, β, γ (degrees) = 41.9, −159.8, 15.8. Experimental conditions: microwave frequency, 14,975 MHz; microwave power, 0.12 mW; modulation amplitude, 0.6 mT (6 G); modulation frequency, 100 kHz; temperature, 20 K. The P-band spectrometer has been described before (9).

To maintain the accuracy of the simulated spectrum, the standard for the permissible rippling is determined by the signal-to-noise ratio. The signal intensity is defined as the difference between the maximal positive and the maximal negative amplitude of a spectrum. This definition can be applied to the difference spectrum of mosaic rippling to obtain the simulation-noise intensity and to an experimental spectrum to obtain the experimental-noise intensity. The number of orientations is determined by the requirement that the S/N ratio of the simulation not exceed the S/N ratio of the experimental spectrum. The solid circles in Fig. 2 give the relation between the S/N ratio and the number of computed orientations.

An experimental metalloprotein EPR spectrum of extremely high quality has a S/N ratio on the order of 200 to 250 so that about 8100 orientations ($m_\theta = 91$ and $m_\phi = 89$) must be computed. Frequently, experimental S/N ratios much lower than 250 are encountered, which allows the number of orientations to be reduced with no loss of accuracy. For S/N ratios of 100, 40, and 16, the allowed reductions decrease the computation time by factors of 1.5, 2.0, and 2.8, respectively.

The powder loop must be constrained so that σ_g does not become approximately equal to zero (the normalized line shape function will have infinite amplitude). To avoid this problem, a zero-width protector equal to one interval of the spectral x-axis mesh is added in quadrature to σ_g. The zero-width protector contributes an insignificant artificial broadening to the spectrum.

TABULATION OF THE LINESHAPE FUNCTION

In the inner loop of the integration, the computation of the exponential function associated with most shape functions (e.g., a normal distribution) is particularly time-consuming. This time can be significantly reduced by using a tabulated shape function. This numerical approximation does not affect the accuracy of the simulation provided the table is sufficiently large. Using a symmetrical shape function in g space allows this table to be folded about zero, which reduces the storage required by a half. If the table mesh is one-fifth that of the x-axis scan (i.e., about 10^3 entries), the tabular error is an order of magnitude smaller than the x-axis stepwidth for all lines that are not wider than the x-axis scan. We find a decrease in computation time by a factor of 3.9.
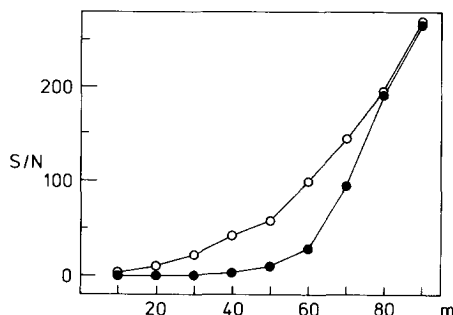

FIG. 2. S/N ratio of rippling simulations as a function of the number of molecular orientations $m_\theta = m + 1$ and $m_\phi = m - 1$ with respect to a near-ideal simulation with index $m = 300$. (●) Unfiltered data; (○) optimally Fourier-filtered data. The graph can be used to determine the minimal number of orientations needed to simulate an experimental ferredoxin spectrum of given S/N ratio.

It must be noted that in some computing systems, the floating-point to integer conversion associated with the use of tabular data may also be a time-consuming operation, particularly when implemented in a higher-level language. To avoid this difficulty, the x-axis mesh may be integerized provided that the size of the table is increased to compensate for the resulting error propagation or that the mesh point is periodically corrected to eliminate the error propagation. In our case, the computation time is further decreased by a factor of 2.1.

HIGH-FREQUENCY TRUNCATION AND DIFFERENTIATION IN FOURIER SPACE

In g-strained spectra, mosaic rippling stems predominantly from near zero-strain orientations, i.e., intermediate orientations for which the linewidth is much smaller than the width along the principal g-tensor axes. The mosaic ripples can be distinguished from the gross features of the ideal simulation by their width so that, in Fourier space, truncation of the high-frequency part filters the ripples.

As an example, Fig. 3 gives the "absolute Fourier transforms" of the two simulations of Fig. 1. The bulk of the EPR information can be seen to be contained in the first 30 channels of the 129-channel absolute Fourier transform, while the ripple structure appears in the intermediate channels. The effect of increasing the truncation channel, K, on the back-transformed simulation is illustrated in Fig. 4.

As before, a S/N ratio is defined for the filtered spectrum with respect to an ideal, unfiltered simulation. To analyze the efficiency of the filtering, Fig. 5 contains plots of the S/N ratio as a function of the truncation channel K for different values of m. Several observations based on Fig. 5 are pertinent: (1) the S/N ratio is a monotonically increasing function of m; (2) truncation within the first few tens of channels causes a very rapid loss of EPR information; (3) at the edge of this area the S/N ratio rises steeply to a maximum; and (4) this edge increases slowly with m.

Filtering in Fourier space gives the most striking results when the experimental S/N level allows the simulation to be based on a relatively low value of m. S/N
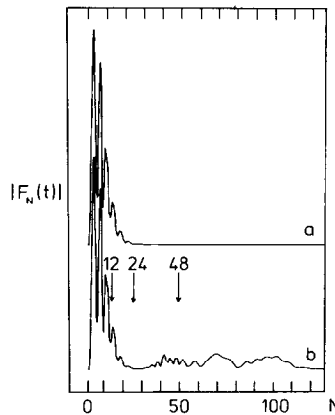

FIG. 3. Absolute value of the Fourier transforms of the two spectra in Fig. 1. The near-ideal simulation is essentially zero for channel numbers greater than 30, while the rippling simulation has significant intensity at intermediate channel numbers. Arrows indicate truncation channels for the corresponding real-space spectra in Fig. 4.
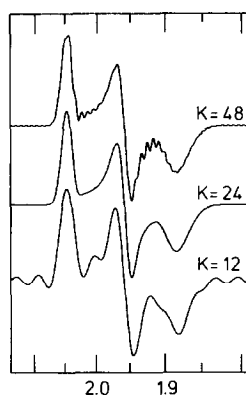
FIG. 4. Effects of Fourier filtering on rippling simulation (256 points; 41 × 39 orientations). The filtering is suboptimal for the first trace, optimal for the second, and overdone (i.e., eroding the EPR information) for the last.

ratios for optimal filtering, the open circles, are included in Fig. 2. As shown, Fourier filtering allows a further reduction in the number of computed orientations with no decrease in the S/N ratio. For S/N ratios of 100, 40, and 16, filtering reduces the computation time by factors of 1.4, 2.5, and 4.5, respectively.

In addition to an effective filtering of high-frequency components, the excursion in Fourier space provides an easy method for differentiating the spectrum (10), which is necessary when the simulation is computed in g space rather than in B space. An advantage of working in g space is that the lineshape is symmetric, which reduces the length of the computation by half. Subsequent transposition and renormalization in B space is most conveniently carried out with the absorption spectrum.

PROGRAM OVERVIEW AND EVALUATION

The techniques outlined above for the computation of g-strained spectra yield an efficient simulation program consisting of the following steps:
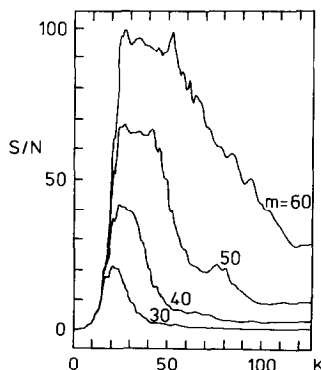

FIG. 5. Plot of the S/N ratio of Fourier-filtered simulations as a function of the truncation channel. Optimal filtering occurs when the truncation channel is chosen to correspond to the maximum of the appropriate trace.

(1) Tabulation of the line shape function if necessary;

(2) Based on the values for the 4×3 spectral parameters (g_1, g_2, g_3, σ_1, σ_2, σ_3, r_{12}, r_{23}, r_{13}, α, β, and γ) compute the rotation matrix and the coefficients in the equations for the resonance position, intensity, and width (cf. Eqs. [2]–[6]);

(3) Integrate over the surface of the unit sphere, i.e., for each molecular orientation, compute the actual values of Eqs. [2]–[6] and the shape function, which is obtained from the tabular data;

(4) Transpose to field space, i.e., renormalize the area under the absorption curve and correct the transition probability by the factor dB/dv;

(5) Transform the spectrum to Fourier space (using the FFT algorithm), apply the high-frequency filter (chopping) to reduce mosaic rippling, differentiate in Fourier space, and back-transform.

To illustrate this program, we have used the simulation of a simple, single-component $S = \frac{1}{2}$ spectrum with only a linewidth due to g strain (e.g., with no hyperfine interactions). The generation of this spectrum (Fig. 1) consumes about 0.3 s on an Amdahl 5860 and about 5 s on a DEC VAX 11. The time required to simulate multicomponent spectra is proportional to the number of components. The presence of resolved hyperfine structure increases the computation time in proportion to the product of the multiplicities of all interacting nuclei. Minimization requires on the order of 10^3 simulations. Accurate reduction of metalloprotein EPR data, based on sophisticated theory, requires simulation programs at least as fast as the program outlined above.

Previously, a common approach to simulate powder EPR spectra has been to make the ad hoc assumptions of a linewidth tensor collinear with the g tensor and an inhomogeneous lineshape that is symmetrical in field space (c.f. Refs. (2, 3)). This technique may prove fruitful if its limitations are kept in mind. For example, if spin quantitation of an $S = \frac{1}{2}$ signal is hampered by low signal-to-noise levels, quantitation of an approximative simulation can be a reasonable alternative. The quality of this "dummy" (i.e., not theoretically founded) fit may be improved by simply summing a number of different symmetrical fits to account for asymmetries in actual spectra. Contrary to widespread belief, however, "deconvolution" of complex spectra from multicenter metalloproteins on basis of this technique does not necessarily result in facts of any significance on, e.g., the stoichiometry of prosthetic groups. On the other hand, our theory and data-reduction techniques provide, for the first time, a practical means to analyze these multicomponent spectra in a rigorous manner.

It may be objected that the quality of our simulations is high simply because our general model allows for more free parameters to be fit than the common ad hoc approaches do. Although this statement is formally correct, in practice we anticipate the opposite to be true for most classes of metallo-proteins. Our present analysis of the spectrum of a [2Fe–2S] ferredoxin, as well as our previous approximative analyses of the spectra of a cytochrome (8) and another [2Fe–2S] ferredoxin (11) indicate that full correlation between all variables of the p tensor is the rule rather than the exception. Consequently, the r_{ij}'s in Eq. [6] are no longer free parameters or, alternatively, Eq. [25] in the accompanying paper can be replaced by the simpler Eq. [34]. Thus, we have three g values and six linewidth parameters to be fit. The ad hoc approach uses three g values and three linewidth parameters, but it is unable

to quantitatively simulate the spectra of [2Fe–2S] ferredoxins or low-spin ferric cytochromes as a single system. The next least complicated step would be to simulate the spectra as a sum of two (or more) single signals. This increases the number of parameters to thirteen (or more), namely, six g values, six linewidth parameters, and a weighting factor. Of course, the artificially introduced multiplicity also makes the fit less significant from a (bio)chemist's point of view. Therefore, our method is not only superior because it is theoretically well founded, but also numerically because it requires less free parameters, at least for the few spectra that have been scrutinized thus far.

APPLICATIONS: THE Fe/S CENTERS IN NADH:Q OXIDOREDUCTASE AND IN QH$_2$:FERRICYTOCHROME c OXIDOREDUCTASE[1]

The following two examples were chosen as typical cases in which a more sophisticated analysis of EPR data can provide important insight into biochemical problems, where the ambiguous results of common, ad hoc analyses have led to ongoing controversies.

NADH:Q oxidoreductase (EC 1.6.99.1) from bovine-heart mitochondria contains a single FMN molecule and four different NADH-reducible iron–sulfur centers, labeled N-1 through N-4. Orme-Johnson et al. originally estimated these centers to be present in an approximate 1:1:1:1 stoichiometry, on the basis of direct integration of EPR (difference) spectra (12). However, computer simulations and integrations by Albracht et al. (13) indicated a stoichiometry for centers N-1:N-2 of 0.5:1 and, possibly, also a less than unit ratio for centers N-3:N-2. These observations triggered a discussion on the question whether a dimeric complex, containing a single center N-1 and, possibly, a single center N-3, should be considered to be the minimal functional unit of this enzyme or, alternatively, whether the preparations are inhomogeneous, containing two—possibly functionally different—entities, namely, one containing centers N-1, N-2, N-3, N-4, and one containing centers N-2, N-4 (cf. Ref. (3) for a review). As a further complication, Ohnishi et al. (14) reported a center N-1 concentration of 0.8 per FMN where Albracht et al. found 0.4 N-1 per FMN (13). Also, Hagen determined an N-1/N-2 ratio close to unity in membrane fragments from Paracoccus denitrificans and from pigeon-heart mitochondria (15). Thus, the question arises whether the inconsistencies might be rooted in the method of EPR data analysis, instead of in the existence of a unique NADH:Q oxidoreductase in bovine-heart mitochondria.

We have simulated the spectrum of NADH-reduced NADH:Q oxidoreductase as a sum of four g-strained $S = \frac{1}{2}$ systems of equal concentration. To keep this multivariable problem tractable, we have assumed the p-tensor elements to be fully correlated. As the initial parameter set we have taken the published (13, 14) g values and linewidths, where we have converted the latter from field units to g-value units, to be substituted on the diagonal of the p tensor in Eq. [34] of the preceding paper. We have subsequently minimized repeatedly on the four individual spectral components, the result being given in Fig. 6. This fit is not necessarily unique; it is based on several simplifying assumptions. It is not certain whether full

---

[1] Abbreviations used: NADH, reduced form of nicotinamide adenine dinucleotide; Q, ubiquinone; FMN, flavin mononucleotide.
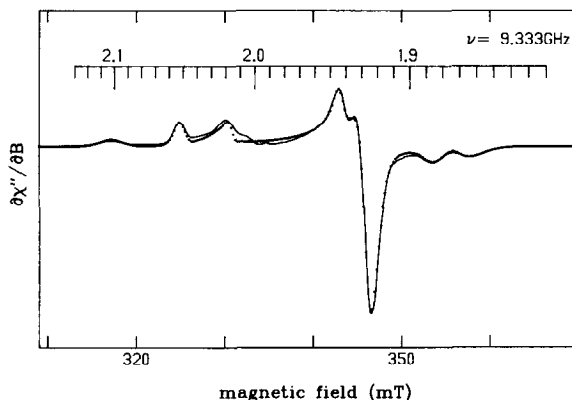
FIG. 6. The spectrum (solid trace) of NADH-reduced NADH:Q oxidoreductase, simulated as the equimolar sum of the four iron–sulfur centers N-1 through N-4. Simulation parameters (61 × 61 orientations) for center N-1: $g_{1,2,3}$ = 1.925, 1.937, 2.019; $\Delta g_{11,22,33,12,13,23}$ = 0.0038, 0.0081, 0.0068, 0.0015, −0.0016, −0.0007; center N-2: g_i = 1.925, 1.925, 2.053; Δg_{ij} = 0.0058, 0.0050, 0.0044, 0.0000, 0.0045, −0.0024; center N-3: g_i = 1.887, 1.941, 2.103; Δg_{ij} = 0.0071, 0.0030, 0.0114, 0.0000, 0.0000, 0.0000; center N-4: g_i = 1.862, 1.921, 2.034; Δg_{ij} = 0.0103, 0.0061, 0.0112, −0.0027, −0.0071, 0.0026. Experimental conditions: microwave frequency, 9333 MHz; microwave power, 0.2 mW; modulation amplitude, 1.25 mT; modulation frequency, 100 kHz; temperature 15 K.

correlation is a valid limitation; three of the four clusters are possibly [4Fe–4S] clusters (cf. Ref. (*3*)) for which no rigorous model simulations have been carried out as yet. Also, the linewidth of the individual components is slightly dependent on the microwave frequency (*16*) indicating some contribution from ligand hyperfine interactions, which may considerably increase the number of parameters to be fit.

Although the analysis of Fig. 6 may not have uniquely pinned down the Zeeman interaction and the *g* strain in centers N-1 through N-4, it does show that at least one nearly perfect fit to the data can be obtained assuming *equal* concentration for all four centers (note: the simulation does not include the partly saturated radical signal around *g* = 2 from FMN and/or ubiquinone). If anything, the stoichiometry of the centers N-1 and N-3 could be slightly higher than unity, but not lower. Previously, the shape of the derivative-type feature around *g* = 1.92–1.94 was taken as evidence, by spectral simulation, that the intensity of center N-1 was only half that of the other centers (*13*).

In summary, to obtain a good fit to the complete spectrum of NADH:Q oxidoreductase, one does not have to abandon the minimum hypothesis of unit stoichiometry for all four iron–sulfur centers. Thus, it seems to us that the discussion on a more complicated enzymic unit may have been initiated prematurely, based on an ill-defined concept of inhomogeneously broadened EPR.

The second example of a controversial biochemical result, whose ambiguity may be resolved by a *g*-strain analysis, comes from the EPR of the enzyme ubiquinol:ferricytochrome *c* oxidoreductase (EC 1.10.2.2). In addition to three cytochromes this protein complex contains a [2Fe–2S] ferredoxin, commonly known as the Rieske protein. When the enzyme is partially reduced with excess sodium ascorbate, the Fe/S center exhibits a very characteristic EPR signal in such widely diverse tissues as beef heart (*17*) and *P. denitrificans* (*18*). De Vries *et al.* have

sought to explain the typical inflection points and asymmetries of this spectrum, by means of an ad hoc simulation, as an approximately equimolar sum of two symmetrical spectral components (*17*). Based on this and other observations, they proposed an intricate model for electron transfer through QH_2:cytochrome c oxidoreductase (*19*) in which the minimal active unit of the enzyme is a structurally, as well as functionally, asymmetric dimer (i.e., one containing two discernible ferredoxins as well as six discernible cytochromes). Subsequently, several authors (*3, 15, 20, 21*) pointed to the possibility that the failure to simulate the Rieske EPR signal as a single $S = \frac{1}{2}$ spectrum, may simply reflect the ad hoc approach falling short of describing line broadening in ferredoxins. The biochemical implication of this suggestion is that there is only one Rieske center and that its EPR does not support the notion of any dimeric complex.

We have attempted to simulate the Rieske spectrum as the signal of a single, magnetically isolated, g-strained $S = \frac{1}{2}$ system. We have used the most general expression for the g strain. In addition, we have modeled a small contribution to the linewidth from unresolved ligand hyperfine interactions by replacing the isotropic residual broadening with a three-dimensional tensor collinear with the g tensor. This boosts the total number of free parameters to be fit up to fifteen for a single center. The result of extensive minimization is presented in Fig. 7. The fine details of the spectrum are *not* faithfully reproduced. Most notably, the highly characteristic and reproducible deflection at $g^{\text{eff}} \simeq 1.78$ is not simulated. This result strongly suggests that the Rieske spectrum does not represent a single isolated center, and that relevant biochemical information is indeed contained in the spectral particulars. The misfit does not necessarily imply that the spectrum is a sum of two (or more) signals from two (or more) noninteracting centers, since restricting the analysis to data taken at a single microwave frequency, makes it impossible to check for magnetic interactions, such as spin coupling to another paramagnetic center in the complex. A multifrequency EPR study is underway to discriminate between these possibilities.
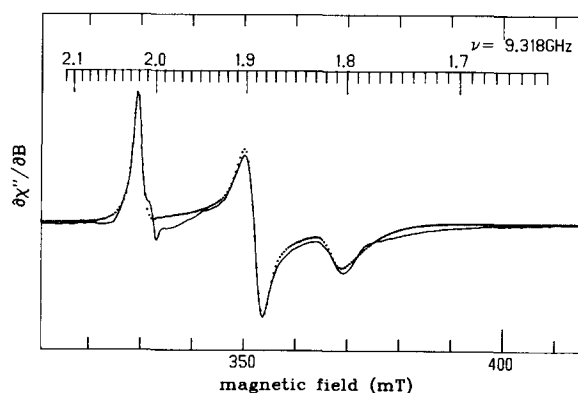

FIG. 7. The spectrum (solid trace) of ascorbate-reduced QH_2:ferricytochrome c oxidoreductase, simulated as a single, noninteracting $S = \frac{1}{2}$ system. Simulation parameters (81×61 orientations): $g_{1,2,3} = 1.789$, 1.891, 2.021; $\alpha_{1,2,3} = 0.0228$, 0.0078, 0.0579; $r_{12,23,31} = -1.00$, -1.00, 0.97; α, β, $\gamma = -158.2$, 53.1, -10.0. Experimental conditions: microwave frequency, 9318 MHz; microwave power, 2 mW; modulation amplitude, 0.63 mT; modulation frequency, 100 kHz; temperature, 36 K.

The two examples treated above illustrate that the fine details of powder EPR spectra can contain valuable information that is easily lost or misinterpreted when the data are "analyzed" by means of simulators based on algorithms of insufficient theoretical foundation. We contend that the methodology and theory put forth in this and in the accompanying paper, set new standards of quality for the interpretation of EPR in distributed systems, which may be quite laborious to apply, but which pay off in the long run, cutting short any tendency to overinterpret complicated EPR spectra with irrelevant paper chemistry.

REFERENCES

1. W. R. HAGEN, D. O. HEARSHEN, R. H. SANDS, AND W. R. DUNHAM, submitted.

2. R. AASA AND T. VÄNNGÅRD, *J. Magn. Reson.* **19**, 308 (1975).

3. H. BEINERT AND S. P. J. ALBRACHT, *Biochim. Biophys. Acta* **683**, 247 (1982).

4. F. K. KNEUBÜHL, *J. Chem. Phys.* **33**, 1074 (1960).

5. J. A. IBERS AND J. D. SWALEN, *Phys. Rev.* **127**, 1914 (1962).

6. A. ISOMOTO, H. WATARI, AND M. KOTANI, *J. Phys. Soc. Jpn.* **29**, 1571 (1970).

7. L. H. STRONG, Ph.D. thesis, University of Michigan, 1976.

8. W. R. HAGEN, *J. Magn. Reson.* **44**, 447 (1981).

9. W. R. DUNHAM, R. H. SANDS, R. W. SHAW, AND H. BEINERT, *Biochim. Biophys. Acta* **748**, 73 (1983).

10. E. O. BRIGHAM, "The Fast Fourier Transform," Prentice–Hall, Englewood Cliffs, N.J., 1974.

11. W. R. HAGEN AND S. P. J. ALBRACHT, *Biochim. Biophys. Acta* **702**, 61 (1982).

12. N. R. ORME-JOHNSON, R. E. HANSEN, AND H. BEINERT, *J. Biol. Chem.* **249**, 1922 (1974).

13. S. P. J. ALBRACHT, G. DOOIJEWAARD, F. J. LEEUWERIK, AND B. VAN SWOL, *Biochim. Biophys. Acta* **459**, 300 (1977).

14. T. OHNISHI, H. BLUM, Y. M. GALANTE, AND Y. HATEFI, *J. Biol. Chem.* **256**, 9216 (1981).

15. W. R. HAGEN, Ph.D. thesis, University of Amsterdam, 1982.

16. S. P. J. ALBRACHT, *Biochim. Biophys. Acta* **347**, 183 (1974).

17. S. DE VRIES, S. P. J. ALBRACHT, AND F. J. LEEUWERIK, *Biochim. Biophys. Acta* **546**, 316 (1979).

18. S. P. J. ALBRACHT, H. W. VAN VERSEVELD, W. R. HAGEN, AND M. L. KALKMAN, *Biochim. Biophys. Acta* **593**, 173 (1980).

19. S. DE VRIES, S. P. J. ALBRACHT, J. A. BERDEN, AND E. C. SLATER, *Biochim. Biophys. Acta* **681**, 41 (1982).

20. B. L. TRUMPOWER, *Biochim. Biophys. Acta* **639**, 129 (1981).

21. J. C. SALERNO, *J. Biol. Chem.* **259**, 2331 (1984).